

Chitin/Metal-Organic Framework Composites as Wide-Range Adsorbent

Gabriel I. Tovar Jimenez,^[a, b] Ainara Valverde,^[c, d] Cristian Mendes-Felipe,^[c, d] Stefan Wuttke,^{*[c, e]} Arkaitz Fidalgo-Marijuan,^[c, f] Edurne S. Larrea,^[g, h] Luis Lezama,^[i] Fangyuan Zheng,^[c] Javier Reguera,^[c, e] Senentxu Lanceros-Méndez,^[c, e] María I. Arriortua,^[c, j] Guillermo Copello,^{*[a, b]} and Roberto Fernández de Luis^{*[c]}

Composites based on chitin (CH) biopolymer and metal-organic framework (MOF) microporous nanoparticles have been developed as broad-scope pollutant adsorbent. Detailed characterization of the CH/MOF composites revealed that the MOF nanoparticles interacted through electrostatic forces with the CH matrix, inducing compartmentalization of the CH macropores that led to an overall surface area increase in the

composites. This created a micro-, meso-, and macroporous structure that efficiently retained pollutants with a broad spectrum of different chemical natures, charges, and sizes. The unique prospect of this approach is the combination of the chemical diversity of MOFs with the simple processability and biocompatibility of CH that opens application fields beyond water remediation.

Introduction

Water is an essential resource for Earth's ecosystems considered at as whole. Any pollution input within the natural water cycle impacts on the base of the trophic chain in the short term, reaching in the long term to affect all its scales. The challenge of the current water remediation lies in the pollution heterogeneity, since in addition to heavy metals or oxyanions derived from natural geologic environments, human activities incorporate uncountable types of inorganic and organic long-term persistent chemicals to the water cycle. Today, highly persistent pollutants such as antibiotics, endocrine disruptors, heavy metals, nanoparticles, organic dyes, and pesticides can be found

in wastewater streams.^[1–3] The wide range of chemical characteristics of these pollutants makes cleaning such a complex matrix an enormous challenge beyond the capabilities of a single technology or material. The development of efficient and broadly applicable water remediation technologies is an urgent need and must consider the fundamental properties of these hazardous molecules, such as their size, shape, charge, and potential binding groups (Figure 1).

Heavy metals, for example, are found as positive, negative, or neutral aquo-oxo-metal species up to 4.5 Å in dynamic diameter. The size, charge, and chemical variety of organic pollutants is even higher. They range from small, Ångstrom-scale molecules (e.g., drugs, endocrine disruptors, or organic

[a] G. I. Tovar Jimenez, Dr. G. Copello
Facultad de Farmacia y Bioquímica, Departamento de Química Analítica y Físicoquímica

Universidad de Buenos Aires (UBA)
Junín 956, C1113AAD, Buenos Aires (Argentina)
E-mail: gcopello@ffyb.uba.ar

[b] G. I. Tovar Jimenez, Dr. G. Copello
Fac. de Farmacia y Bioquímica, (IQUIMEFA-UBA-CONICET)

Instituto de Química y Metabolismo del Fármaco
Junín 956, C1113AAD, Buenos Aires (Argentina)

[c] A. Valverde, C. Mendes-Felipe, Prof. S. Wuttke, Dr. A. Fidalgo-Marijuan, F. Zheng, Dr. J. Reguera, Prof. S. Lanceros-Méndez, Prof. M. I. Arriortua, Dr. R. F. de Luis
BCMaterials, Basque Center for Materials, Applications and Nanostructures UPV/EHU Science Park, 48940 Leioa (Spain)
E-mail: stefan.wuttke@bcmaterials.net
roberto.fernandez@bcmaterials.net

[d] A. Valverde, C. Mendes-Felipe
Macromolecular Chemistry Group (LABQUIMAC), Department of Physical Chemistry, Faculty of Science and Technology
University of the Basque Country (UPV/EHU)
Barrio Sarriena s/n 48940 Leioa, Spain
and
48013 Bilbao (Spain)

[e] Prof. S. Wuttke, Dr. J. Reguera, Prof. S. Lanceros-Méndez
IKERBASQUE, Basque Foundation for Science
48013 Bilbao (Spain)

[f] Dr. A. Fidalgo-Marijuan
Dept. of Organic Chemistry II, Faculty of Science and Technology
University of the Basque Country (UPV/EHU)
Barrio Sarriena s/n 48940 Leioa, Spain
and
48013 Bilbao (Spain)

[g] Dr. E. S. Larrea
Le Studium Research Fellow
Loire Valley Institute for Advanced Studies
45100 Orléans (France)

[h] Dr. E. S. Larrea
CEMHTI – UPR3079 CNRS
1 avenue de la Recherche Scientifique, 45100 Orléans (France)

[i] Prof. L. Lezama
Departamento de Química Inorgánica, Facultad de Ciencia y Tecnología
University of the Basque Country (UPV/EHU)
Barrio Sarriena s/n 48940 Leioa, Spain
and
48013 Bilbao (Spain)

[j] Prof. M. I. Arriortua
Departamento de Geología, Facultad de Ciencia y Tecnología
University of the Basque Country (UPV/EHU)
Barrio Sarriena s/n 48940 Leioa, Spain
and
48013 Bilbao (Spain)

 Supporting information for this article is available on the WWW under <https://doi.org/10.1002/cssc.202100675>


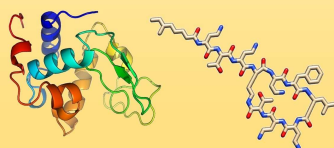
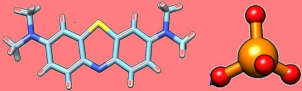
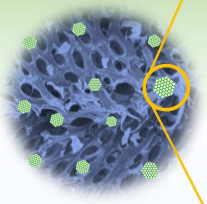
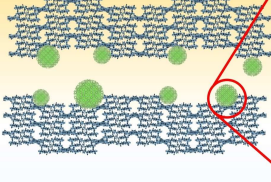
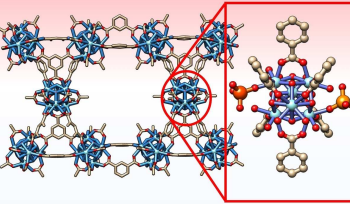
Model Adsorbates			
Nanoparticles	Large-Medium Macromolecules (e.g. Protein) (e.g. Enzymes)	Small Molecules (e.g. Dyes, Drugs)	Metal Ions (e.g. Heavy Metals)
Above 1 nm	1nm - 30 Å	Bellow 30 Å	Bellow 5 Å
 <p>Au NPs 13 nm Negative Electrostatic Interaction</p>	 <p>Lysozyme protein 30 x-45 Å Positive N-acetylmuramic acid N-acetyl-D-glucosamine</p> <p>Polymyxin B 50 x 20 Å Positive Amine, amide, hydroxyl</p>	 <p>Methylene Blue 15 x 5 Å Positive Amine, amide, hydroxyl</p> <p>Chromate anion 4 Å Negative Oxygen/hydroxyl</p>	
CH/MOF-808 Adsorbent			
Macro-pores >500 Å (Chitin Matrix)	Meso-pores 500 – 20 Å (Chitin – MOF-808 surface)	Micro-pores <20 Å MOF-808 structure	
			

Figure 1. Representative examples of organic and inorganic components that can be found in a wastewater stream as well as their possible adsorption by the developed CH/MOF-808 composites at the micro-, meso-, and macropores.

dyes), to nano- (e.g., nanoparticles) and even micron-scale pollutants (e.g., enzymes, hormones, proteins, or micro-plastics). Therefore multi-use water remediation technology must be able to remove a large variety and size-range of pollutants (Figure 1).^[4–6]

Of the current wastewater treatment technologies, adsorption has emerged as a green, efficient, selective, and reusable option.^[7] Many types of different sorbents have been developed and tested to recover single specific pollutants. Nevertheless, this “one adsorbent/one pollutant” strategy does not address the challenge of cleaning real water samples that often contain multiple pollutants.

To achieve broad-scope sorption the sorbent materials should comply with at least two requirements. First, it is necessary to synergistically combine micro-, meso-, and macropores within the sorbent.^[8] Second, functionalization of the porous scaffold is needed, as this enables to introduce host-guest interactions to trap neutral, anionic, and cationic compounds.^[9] Encompassing these characteristics in one sorbent is not straightforward, since well-ordered microporous materials lack the capacity to trap large molecules, whilst macro- and mesoporous polymers usually fail to retain small metal ions.^[10,11]

Therefore, in this work we have combined a macro- and mesoporous chitin (CH)^[12–15] biopolymer with the MOF-808

microporous metal-organic framework (MOF)^[16,25,17–24] sorbent to create a porous composite with multiple porosities and chemical functionalities.^[28–30] CH is the second most abundant natural polymer.^[31,32] It can be easily handled and processed as macro- and mesoporous gel,^[33–36] which enables its use as sorbent for macromolecules (e.g., enzymes and proteins).^[37–40] Nevertheless, CH usually lacks the adsorption affinity for cationic and anionic inorganic species at the microporous scale.^[41] To overcome this challenge, Zr-based MOF-808 nanoparticles have been included as fillers within the CH matrix.^[42,43] MOF-808 has been specifically selected because it exhibits (i) a wide pore window and high surface area ($\approx 2000\text{--}1000\text{ m}^2\text{ g}^{-1}$) that facilitates the pollutant migration into the structure, and (ii) linker defects at the inorganic hexa-nuclear clusters supporting the adsorption of negatively charged inorganic oxyanions and molecules.^[44–49] Moreover, MOF-808 nanoparticles function as a modulator of the CH porosity, leading to a synergistic effect of the adsorption capacity and affinity of CH/MOF-808 composites in comparison to the average sum of their individual components.

Results and Discussion

The synthesis of CH/MOF-808 composites is carried out by a three-step route, as detailed in the Experimental Section (Figure S1). First, MOF-808 nanoparticles are synthesized solvothermally,^[50–52] then they are dispersed in a chitin gel solution, and finally, the composites are processed by wet spinning. Three CH/MOF-808 samples were obtained varying the MOF-808 weight content from 5% (CH 5), 10% (CH 10), to 15% (CH 15). X-ray diffraction (XRD) analyses of the MOF-808 nanoparticles confirm the correlation between the experimental and calculated patterns obtained from the structural model of MOF-808 (Figure 2a, b).^[53,54]

The structural stability of MOF-808 after being incorporated into the CH biopolymer is confirmed in a first visual inspection of the CH/MOF-808 patterns (Figure 2a–c).^[55] The profile matching analysis of CH/MOF-808 XRD data allows semi-quantification of MOF-808 loading in CH5, CH10, and CH15 composites (Figure 2c, d, S2–5).

As shown in the transmission electron microscopy (TEM) images (Figure S6a, b), the presence of water in the synthesis media reduces the MOF-808 particle size from the micron- to the nanoscale (20 ± 4 nm in diameter). No morphological or particle size changes of MOF-808 nanoparticles are produced due to their incorporation into the biopolymer (Figure S6c, d).

The morphology and structure of CH/MOF-808 composites were also studied by scanning electron microscopy (SEM; Figure S6e–l). CH shows a macroporous structure with average

pore diameters of 18 ± 2 μm (Figure S6e). The first consequence of the incorporation of MOF808 nanoparticles is the CH pores compartmentalization to 7 ± 2 μm in CH5 (Figure S6f), $2,3 \pm 1.3$ μm and 640 ± 160 nm for CH10 (Figure S6g), and 1.6 ± 0.7 μm and 450 ± 140 nm for CH15 (Figure S6h). Compositional mapping of carbon, oxygen, and zirconium content in CH/MOF-808 composites (Figure S6i–l) indicates a uniform MOF-808 distribution within the CH structure.

Mercury porosimetry (Figure 3a, b) and room-temperature CO_2 adsorption (Figure 3c, d) measurements were carried out in order to study the porosity of CH/MOF-808 samples from the macro- to the microporous regimes.^[56,57] The macropore compartmentalization directed by the template effect of MOF-808 nanoparticles increases the total porosity and surface area of the samples associated to the macro- and mesopores from $34 \text{ m}^2 \text{ g}^{-1}$ in CH to $275 \text{ m}^2 \text{ g}^{-1}$ in CH15 (Table S1). In addition to the enhancement of the porosity associated to the meso- and macropores, CH/MOF-808 composites also show the microporosity characteristic of MOF-808 nanoparticles (Table S1).^[58]

In order to gain further insights into the interaction between the polymeric CH matrix and the MOF nanoparticles, the CH/MOF-808 composites were studied with different spectroscopic techniques. Raman spectra for MOF-808, CH, CH 5, CH 10, and CH 15 samples are presented in Figure 3e. In MOF-808, the characteristic bands are ascribed to the vibrational modes of inorganic Zr–O bonds (644 cm^{-1}). C–H out-of-plane bending of ring, symmetric stretch (C=C), benzene ring, symmetric stretching (COO), and asymmetric stretch (COO) of

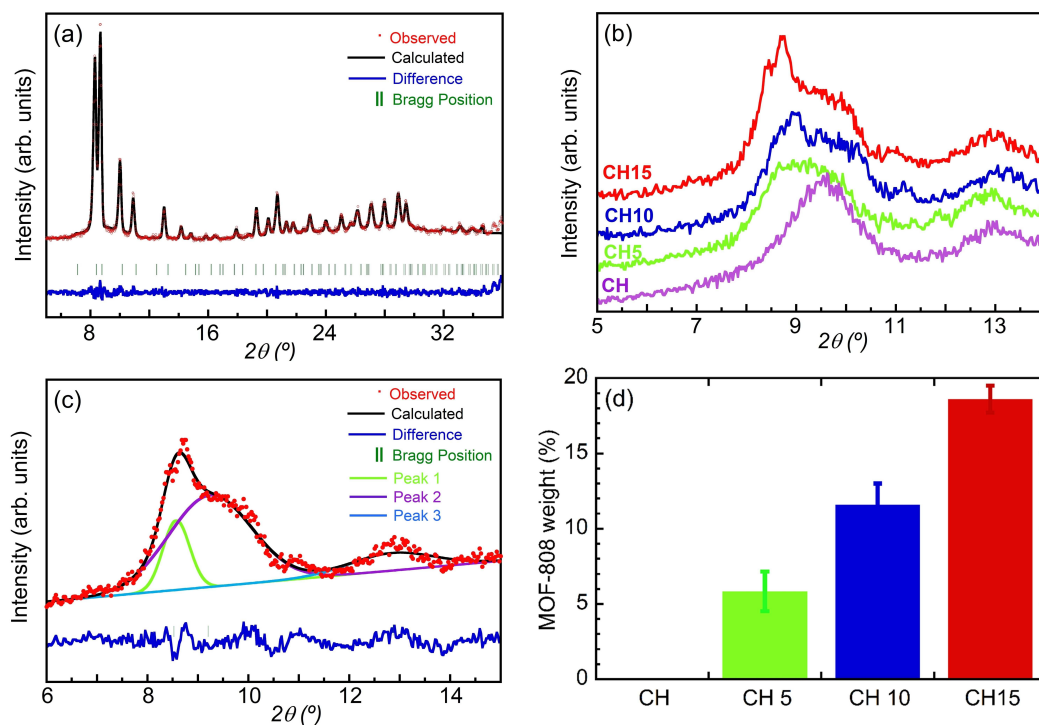


Figure 2. (a) Pattern matching analysis of MOF-808. (b) XRD patterns of CH, CH5, CH10, and CH15. (c) Peak fitting of CH15. (d) Quantification of MOF-808 within CH/MOF-808 composites were studied also by XRD, TEM, and SEM.

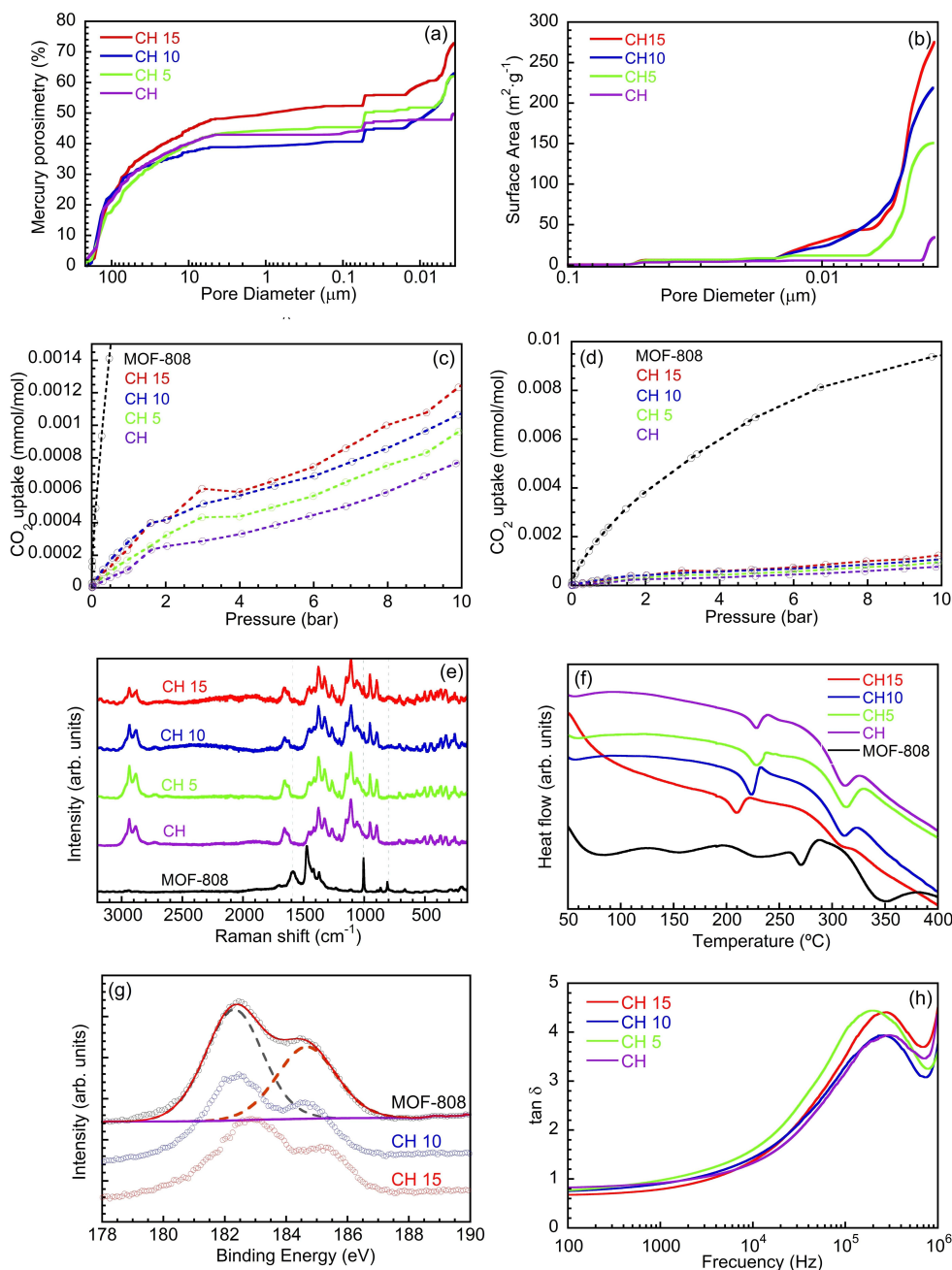


Figure 3. (a) Cumulative porosity variation determined by mercury porosimetry. (b) Cumulative surface area determined by mercury porosimetry. (c) Raman spectra, (d) DSC, (e) XPS, and (f) dielectric relaxation spectra of CH, MOF-808, and composite CH5, CH10, and CH15 samples.

trimesate organic linkers have been also identified at 808, 1008, 1370, and 1473 cm^{-1} , respectively. Spectra for CH/MOF-808 composites reveal predominantly the adsorption bands related to the vibrational modes of the CH matrix. Specifically, Amide I (1630 and 1660 cm^{-1}), Amide III (1200–1350 cm^{-1}), C–O–C and C–O stretching vibration region (1200–950 cm^{-1}), and β -glycosidic bonds (890 cm^{-1}) have been identified as the main Raman fingerprints of CH. The intensity of the 1008 cm^{-1} adsorption band in CH/MOF-808 composites is correlated to the degree of

MOF-808 loading. No meaningful wavenumber displacements or new vibration modes were observed in the Raman signals of the separate components that form the composites, suggesting that the blending of MOF-808 and CH is not based on strong chemical interactions.

The differential scanning calorimetry/thermogravimetric analysis (DSC-TGA) thermograms of pure CH and CH/MOF-808 composites are illustrated in Figure 3e and S7. The TGA curves of CH/MOF-808 show the first weight loss at low temperatures

(RT – 100 °C); associated with the release of adsorbed water molecules. After dehydration, the TGA and DSC curves show a decrease in the temperature of the CH exothermic transition from 250 (CH) to 220 °C (CH 15). This effect is attributed to a reduction of the interactions between CH–CH chains (i.e., increase of the disorder degree) rather than to new chemical interactions with MOF-808 nanoparticles.^[59] At higher temperatures, the CH exothermic deacetylation process starts around 320 °C, which is not altered by the presence of the MOF-808 nanoparticles. The results obtained from X-ray photoelectron spectroscopy (XPS) confirm the conclusion drawn from Raman spectroscopy (Figures 3g and S8). The XPS spectra of CH and CH/MOF-808 composites show the binding energies of CH for O 1 s, N 1 s, and C 1 s. In the specific case of the CH/MOF-808 samples, additional bands related to the Zr 3d_{5/2} (182.2 eV) and Zr 3d_{3/2} (182.9 eV) binding energies have been detected. No significant displacement of the signals is observed after comparing the XPS spectra of MOF-808 with the CH/MOF-808 composites, further confirming that there are no strong interactions between the filler and the polymeric matrix. The dielectric relaxation spectra for all CH/MOF-808 composites show a loss factor (tan δ) peak between 250–350 kHz (Figure 3h). The tan δ peak shifts to lower frequencies upon the addition of MOF-808, indicating a slowing-down of the relaxation dynamics of CH chains. The embedding of MOF-808 within the CH matrix can induce (i) a disorder in the CH polymeric chains and (ii) CH chain – MOF-808 electrostatic interactions, both leading to a decrease the polymer relaxation dynamics.^[60]

Initial adsorption screening tests have been performed with CH, MOF-808, and CH/MOF-808 composites over cationic, anionic, and neutral pollutants with sizes ranging from nano-

meter to the Ångstrom scales. To this end, CH/MOF-808 adsorption efficiency over aqueous solutions of lysozyme (LYS), gold nanoparticles (AuNP, 50 ppm), polymyxin B (POL-B), erythrosine (ERY, 50 ppm), methylene blue (MB, 50 ppm), methyl orange (MO, 50 ppm), Cr^{VI} (50 ppm), and As^V (40 ppm) has been quantified. Figure 4a shows the adsorption efficiency in % adsorption of CH/MOF-808 composites, CH, and MOF-808 materials. In order to uncover whether the assembly of CH/MOF-808 composites synergistically combines the individual MOF-808 and CH components, the experimental adsorption efficiency values for CH 5, CH 10, and CH 15 have been compared with those calculated in the plots of Figure 3b–d, respectively. The calculated adsorption efficiencies have been obtained from the sum of the weight-average adsorption capacities of the MOF-808 and CH in CH 5, CH 10, and CH 15 composites. The difference in adsorption % between the calculated and experimental values of CH/MOF-808 composites is defined by the Equation (1):

$$\Delta SE = (SE_{\text{CH/MOF-808}}) - [(SE_{\text{MOF-808}})WP + (SE_{\text{CH}})(100 - WP)] \quad (1)$$

where ΔSE is the difference in adsorption capacity [%], WP is the weight percentage of MOF-808 on CH/MOF-808 samples, and (SE_{CH/MOF-808}) and (SE_{CH}) are the experimental sorption capacities of separate MOF-808 and CH components. The discussion of the results derived from the adsorption tests will be performed in the following order: metal oxyanions, organic dyes, large molecules, and nanoparticles.

Regarding their chemical properties, inorganic cations and oxyanions are the smallest pollutant species, and their

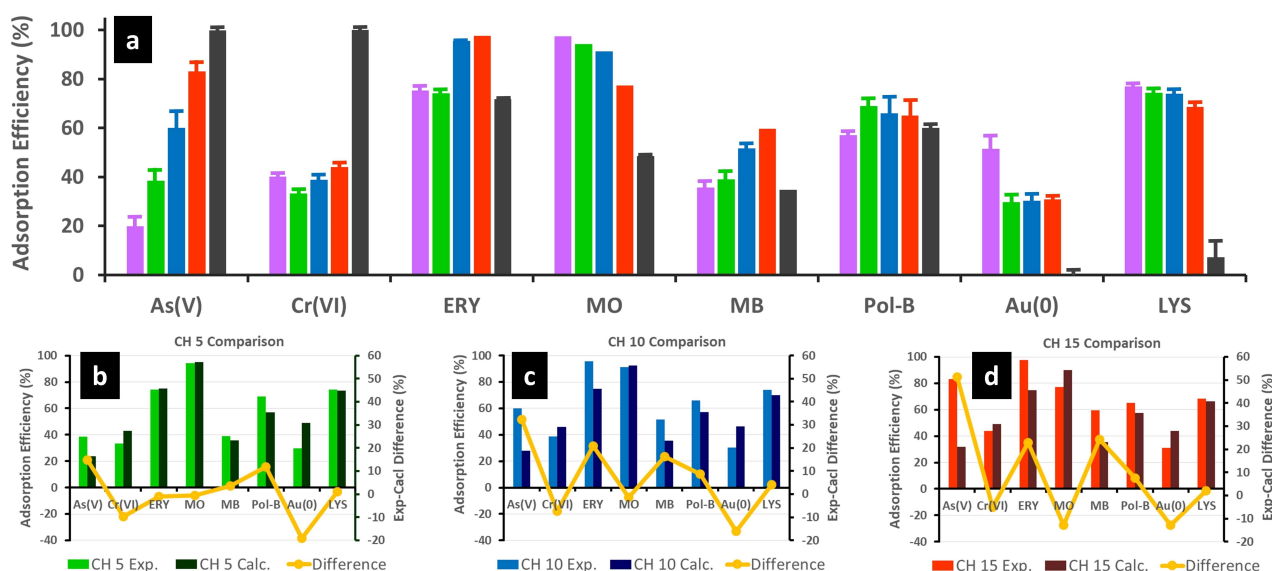


Figure 4. (a) Removal efficiency of CH, CH5, CH10, and CH15 for As^V (40 ppm), Cr(VI) (50 ppm), erythrosine (ERY, 100 ppm), methyl orange (MO, 30 ppm), methylene blue (MB, 100 ppm), polymyxin B (POL-B, 100 ppm), gold nanoparticles (AuNP, 12.5 ppm), and lysozyme (LYS, 5000 ppm). Comparison between experimental (light columns) and calculated (dark columns) adsorption efficiencies for (b) CH5, (c) CH10, and (d) CH15 CH/MOF-808 composites.

adsorption is highly dependent on the presence of attractive charged groups in the adsorbent structure.^[61–63] As demonstrated by previous research,^[42,45,54] MOF-808 shows an As^V removal capacity of near 99% for As^V 40 ppm solution (Figures 4a and S9), while CH exhibits a much lower performance (i.e., 20%). CH/MOF-808 composites show intermediate efficiencies, highly dependent on the MOF-808 content. When comparing experimental and calculated adsorption efficiencies, CH/MOF-808 composites outperform the averaged sum of the capacities of CH and MOF-808 components (Figure 4b–d).

The immobilization of hexavalent chromium anions in MOF-808,^[47,64] CH/MOF-808 composites, and CH matrixes is governed by two factors: (i) adsorption at the CH/MOF-808 structure,^[65–67] and (ii) reduction from Cr^{VI} to Cr^{III} due to the electron donor groups of CH matrix.^[19,68] MOF-808 nanoparticles have a near 100% capacity for the removal of Cr^{VI} species from water; whilst CH and CH/MOF-808 show just a 40% removal. Contrary to the expected tendency, the CH/MOF-808 composites do not show an increase of the chromate anions removal in comparison to CH matrix. In order to gain further insights chromium speciation after operation was studied by means of UV/Vis and electron paramagnetic resonance (EPR) spectroscopies. As revealed by UV/Vis and EPR studies (Figures S10–12), MOF-808 immobilizes chromium mainly as hexavalent chromate and also as highly reactive and hazardous pentavalent chromium (Figure S12a,b). Although CH is less efficient in adsorbing Cr^{VI}, it is highly effective in immobilizing it as trivalent chromium (Figure S12c,d). Similar Cr^{VI}-to-Cr^{III} reduction capacity is found for CH/MOF-808 composites. It seems that the Cr^{VI}-to-Cr^{III} reduction in CH composites is the process that governs the final chromate removal capacity of the system, prevailing over, or even blocking, the Cr^{VI} adsorption process on the MOF-808 nanoparticles. Even though CH and CH/MOF-808 composites are less efficient than MOF-808, and lower than the expected average sum of their capacities (Figure 4b–d), they immobilize the chromium in its less toxic, reactive, and mobile trivalent ion form.

Further, the possibility of removing larger organic molecules was also evaluated for CH/MOF-808 composites. Several organic dyes were first selected with shapes and average dimensions suitable matching MOF's pores^[70] but also having charged groups prone to interact with the CH and CH/MOF-808 surface (Figure 1).^[69] A screening of the CH/MOF-808 adsorption over cationic MB, anionic ERY, and MO dye molecules was carried out (Figure 4). For MO, CH shows higher adsorption capacity (100%) than MOF-808 (50%), and the performance of the CH/MOF-808 composites simply averaged the performances of the individual materials. (Figure 4b–d). Surprisingly, the results obtained for cationic and anionic MB and ERY indicate that CH/MOF-808 composites adsorb them more efficiently than the corresponding MOF-808 or CH components (Figure 4b–d). Two factors could explain this synergetic effect that leads to enhances adsorption of CH/MOF-808 composites: (i) the increase of the active total porosity due to the compartmentalization of the CH macropores into mesopores (i.e., the increase of available surface area), and (ii) the role of the CH/MOF-808 interface.

Further, the behavior of CH/MOF-808 was investigated with respect to the adsorption of larger molecules able to enter the meso- and macroporous structure of CH, but not into the pore system of the MOF-808 nanoparticles. It is worth noting that even if the pore window of the MOF-808 nanoparticles impedes the access of bulky macromolecules within its structure, their outer surface also represents an important adsorption region, since under-coordinated inorganic clusters and organic linkers can act also as interacting points for adsorbates. This is in fact observed for the absorption of POL-B.^[69] Nearly 60% of POL-B molecules are retained at the surface of MOF-808 nanoparticles; a capacity slightly higher than the one observed for the CH macroporous matrix (58%) (Figure 4a). Again, CH/MOF-808 composites outperform the adsorption capacity of the separate CH and MOF-808 components. This behavior further confirms the relevance of the compartmentalization and interface chemistry of CH/MOF-808 porous structure on its adsorption capacity (Figure 4b–d). It is worth noting that POL-B is a natural antibiotic agent used in this work as a model pollutant, since its chemical structure and molecular size resembles the ones of medium molecular size pollutants found in current wastewater, such as hormones or antibiotics.^[3,69]

Due to the meso- and macroporous structure of CH and CH/MOF-808 composites, they are also able to retain larger adsorbates, such as lysozyme^[70,71] protein (30×50 Å) or gold nanoparticles with 13.6±1.4 nm average diameters (Figures S13 and S14). The estimation of an adsorbent system to retain large proteins is also interesting, since, although proteins are not pollutant per se, they are involved in the selective recognition of endocrine disruptor hormones, a property that could lead to future development of CH/MOF-protein systems able to retain them.

MOF-808 is not generally useful in LYS or AuNPs capture, the adsorption capacity for both adsorbates being negligible. In these two cases, the CH macro- and mesoporous structure is the active component, retaining 50 and 70% of gold and LYS, respectively (Figure 4a). For LYS, CH/MOF sorbents show efficiencies slightly lower than CH (Figure 4a), which can be understood as the average sum of CH and MOF-808 (Figure 4b–d). In the case of AuNPs, CH/MOF-808 composites underperform in comparison to their components (Figure 4b–d). For these two case studies, the compartmentalization of the CH macropores into mesopores impede the migration of LYS and AuNPs through the structure of the CH/MOF-808 matrix, reducing the area accessible to the adsorbate. Therefore, compartmentalization of CH macropore structure is beneficial to certain limit in terms of pollutant molecular size. Despite this limitation, it has been duly proved that the synergistic combination of CH and MOF-808 give access to the adsorption of a wide variety of pollutants from the angstrom to nano-regimes.

CH15 composite performance was fully studied for the specific case of pentavalent arsenic oxyanion. It is important to note that arsenic natural pollution is a worldwide issue affecting large geographical areas of many countries (e.g., USA, India, Chile, Argentina, Europe, etc.). As^V adsorption was studied at a 1 ppm initial concentration, which is a level of arsenate contamination common in many river basins worldwide, in

particular in those crossing bedrocks containing arsenic-rich minerals. Full kinetic and isotherm adsorption of As^{V} for the CH15 composite are shown in the Figure 5. The adsorption capacity of the CH15 matrix at 1 ppm arsenic concentration is 33%, far from the 82% value obtained when using a 40 ppm As^{V} concentration (Figure 5a). Nevertheless, at this low concentration, the inclusion of MOF-808 fillers continue to enhance the CH matrix with the affinity for negative species that the CH polymer solely lacks.

The CH15 adsorption kinetic profile for As^{V} (Figure 5b) is similar to that previously reported for zirconium-based MOFs, with most of the adsorption occurring at the first stage of the experiment.^[63] The Elovich model (Table S2), used to fit the experimental data (green line of Figure 5b), indicates that the arsenate is chemisorbed into CH15. This observation is in agreement with previously reported adsorption mechanisms on Zr-MOFs over oxyanions, since it has been experimentally proven that oxyanions uptake occurs through direct coordination of arsenate to the zirconium hexa-nuclear clusters.^[72]

Figure 5c shows the adsorption isotherms for CH15 over arsenate. The data can be fitted with the Freundlich and Langmuir models, resulting in slightly better agreement factors for Freundlich model, (Freundlich, $R^2=0.991$; Langmuir, $R^2=0.958$; Table S2). The values of the q_{max} and k constants (related to the adsorption capacity of the CH15) calculated from the fittings are $10.6 \pm 1.7 \text{ mg g}^{-1}$ and $2.2 \pm 0.2 \text{ mg L}^{-1}$.^[73] More interesting is that the n Freundlich parameter value of 0.39(2) further confirms that a chemisorption mechanism is responsible for arsenate retention within the CH15 composite, overriding the

interparticle interaction effects among the arsenate oxyanions and the CH matrix.

The adsorption capacity of CH15 over As^{V} ($C_0=40 \text{ ppm}$) was also tested in the presence of 40 and 400 ppm sulfate, nitrate, and chloride anions (Figure 5d and Table S4). Figure S15 summarizes the same information but in terms of As^{V} adsorption efficiency. The competition of these anions for the adsorption sites does not strongly affect the performance of CH15. Indeed, the observed deviation is correlated with slight differences of the As^{V} initial concentration found for the solutions containing different competitor species. In the worst-case scenario, a slight reduction of the retention capacity is observed in the presence of 400 ppm of Cl^- and NO_3^- species.

In the specific case of organic dyes, adsorption kinetics for larger molecules is faster than those reported for arsenate oxyanions (Figures S16–18). Indeed, the system reaches equilibrium in 60 min for MB and MO and in 100 min for ERY. The charge of the organic dyes is a key factor in an electrostatic interaction driven adsorption process. In comparison to As^{V} , here the CH plays also a very active role during adsorption, since it is able to retain the same quantity of target dye as MOF-808 (Figure S18).

The presence of MOF-808 after adsorption is confirmed by applying the XRD peak fittings approximation. Nevertheless, post-operation XRD analyses for CH 15 samples after arsenic and dye adsorption suggest that MOF-808 crystallinity decreases during the process (Figures S19–S22). Although the water stability of zirconium-based MOFs is well established,^[53,74] the presence of anionic species in the water matrix, especially

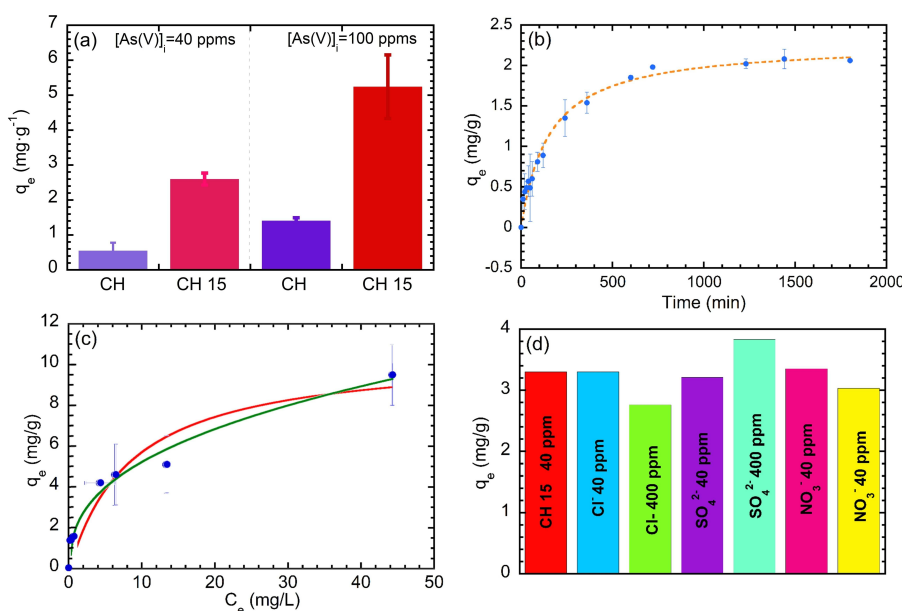


Figure 5. (a) Adsorption capacities over As^{V} at 40 and 100 ppm for CH and CH15. (b) Adsorption kinetics of As^{V} at 1 ppm for CH15 composite. (c) Adsorption isotherm over As^{V} for CH15 (red line: fitting obtained with a Langmuir model, green line: fitting obtained with a Freundlich model). (d) Adsorption capacity over As^{V} ($C_0=40 \text{ ppm}$) of CH15 in the presence of competitor anions at 40 and 400 ppm. The first red colored bar of the Figure 5d is the adsorption capacity of CH15 over As^{V} ($C_0=40 \text{ ppm}$). This data has been depicted as a reference. All the adsorption studies were performed with the addition of 10 mg of CH and CH/MOF composites to 10 mL of arsenic solution.

after a prolonged contact with the MOF structure, can induce a partial displacement of the trimesate organic bridges leading to the partial amorphization of the crystal structure.

IR spectra do not give further information about the MOF-808 degradation process, and neither do the arsenate adsorption mechanisms, since the fingerprint signals for MOF-808 and CH matrix remain unaltered (Figure S23).

Dielectric spectroscopy measurements were performed after the arsenate uptake for CH15 (Figures S24–S27). Arsenate incorporation within CH15 modified the electrical properties of all the composites, lowering electrical conductivity and electrode polarization contribution. This initial evidence directly countered the expected result, since the higher the ionic concentration of water encapsulated within the CH/MOF-808 composite should lead to higher conductivity in the system, unless the arsenate ions are strongly attached to the matrix during adsorption. Indeed, the electrical permittivity increases at low frequencies, and the permittivity slope changes after arsenate uptake, suggest that arsenate is covalently bonded to the CH/MOF-808 matrix. This observation agrees with the Zr binding energy displacement observed in the XPS spectra after the As^V adsorption (Figures S28–S32). The covalent anchoring of arsenate species through Zr–O–As bridges influences the binding energies associated with Zr and oxygen atoms within the zirconium hexa-nuclear clusters.

Conclusion

Metal-organic framework MOF-808 nanoparticles incorporation into chitin (CH) gel polymeric matrix developed micro-, meso-, and macroporous composites that can be used as broad-scope adsorbents. This is possible because MOF-808 nanoparticles compartmentalize into the macroporous structure of CH polymeric matrix, endow the composite with the inherent microporosity of the MOF-808 material itself, and additionally increase the surface area available for absorption.

Due to their micro-, meso-, and macroporous structure, the CH/MOF-808 composites are able to work efficiently for the adsorption of a large variety of pollutants ranging from small ions and molecules to large proteins or nanoparticles. CH/MOF-808 composites exhibit the chemical affinity of their separate components; however, in some cases (e.g., As^V, methylene blue, erythrosine, and Polymyxin B), the material benefits from the synergistic interactions of its components, outperforming both MOF-808 and CH efficiency. This synergetic effect is attributed to (i) the compartmentalization of the CH macropores when including MOF-808 nanoparticles within its structure, and (ii) the active role of the interface between MOF-808 and CH during adsorption. CH/MOF-808 composites are also able to work efficiently in terms of capacity and kinetics over As^V capture in solutions mimicking real polluted waters. As concluded from the fittings of adsorption isotherms and kinetic curves, as well as from the dielectric response of CH/MOF-808 after operation, As^V is captured through chemisorption at the MOF-808 nanoparticles.

Considering the performance of the CH/MOF-808 systems, it can be concluded that we have achieved a broad adsorption technology able to work in the presence of a complex variety of pollutants that can be found in current water streams. Moreover, the MOF structural diversity and designability at the molecular level, combined with the easy processability and biocompatibility of CH polymers, makes the developed materials suitable for applications where available surface area, pore size, and pore chemistry become relevant issues.

Experimental Section

Synthesis of MOF-808 nanoparticles: MOF-808 nanoparticles were synthesized using a slightly modified version of the protocol presented in Ref. [75]. ZrCl₄ (0.1234 g, 0.5295 mmol), 1,3,5-benzenetricarboxylic acid (H3BTC, 0.1237 g, 0.5887 mmol), formic acid (12 mL), water (0.5 mL), and *N,N*-dimethylformamide (DMF, 12 mL) were mixed, stirred at room temperature, sealed in a 25 mL glass autoclave (Schott, Duran®), and then placed in an oven at 120 °C for 48 h. After the reaction, the vessel was cooled naturally to room temperature in the oven. The white precipitate was centrifuged and washed with methanol three times. Subsequently, the obtained precipitate was dried at 80 °C.^[76]

Synthesis of CH and CH/MOF-808 composites: Chitin gels were synthesized according to Ref. [77]. Firstly, calcium solvent was prepared by suspending CaCl₂·2H₂O (42.5 g, 0.288 mol) in 50 mL of methanol and refluxed for 30 min at 82 °C to a state of near-dissolution. Then, 1 g of CH was refluxed in the calcium solvent for 2 h at 90 °C under constant stirring. For the preparation of the composites, 50, 100, or 150 mg of MOF-808 were added to the above solution at this point. This process is illustrated in Figure S1. The mixtures were spinned in methanol until they gelled. Finally, the gel composites were washed three times with methanol overnight. The gel of chitin will be denoted as CH and the obtained composites as CH5, CH10, and CH15, respectively.

Adsorption experiments

Punctual adsorption tests: Adsorption experiments with CH, MOF-808, and CH/MOF-808 were conducted at 20 °C, using 10 mg adsorbent dispersed in 1 mL pollutant model solutions/dispersions contained in a conical flask. The flasks were agitated in vibrator shaker at 180 rpm during 12 h until adsorption equilibrium was reached. After that, the suspension was centrifuged at 6000 rpm for 10 min, filtrated with a hydrophilic 0.20 μm filter, and finally analyzed by means of UV/Vis or inductively coupled plasma atomic emission spectroscopy (ICP-AES) depending on the analyte.

Adsorption kinetic curves: For As^V and some of the organic dyes, the full kinetic and curves were determined by separating the adsorbent and adsorbate solutions at different equilibrium times. To this end, a 1 mL solution of 1 ppm As^V and 100 ppm organic dyes was added to Eppendorf tubes. Afterwards, 10 mg CH15 was added to the solutions. The Eppendorf tube was shaken at room temperature and filtrated at given times of the adsorption process. Measurements were performed in triplicate.

Adsorption isotherm curves: The same experimental protocol was used to determine the adsorption isotherms, but using the same equilibrium time (4 h) and different concentrations of the pollutants in the initial solutions. The adsorbent concentration and volume of the initial solutions were kept as previously described.

Acknowledgements

The authors thank financial support from the Spanish Ministry of Economy and Competitiveness (MINECO) through projects MAT2016-76739-R (AEI/FEDER, EU) and MAT2016-76039-C4-3-R (AEI/FEDER, UE) (including FEDER financial support) and from the Basque Government Industry and Education Departments under the ELKARTEK, HAZITEK and PIBA (PIBA-2018-06) programs, respectively, is also acknowledged. The European Commission Research & Innovation H2020-MSCA-RISE-2017 (Ref.: 778412) INDESMOF project is also acknowledged. The authors thank the technicians of SGIker (UPV/EHU).

Conflict of Interest

The authors declare no conflict of interest.

Keywords: chitin · heavy metals · MOF-808 · sorbents · water remediation

- [1] E. Sanganyado, W. Gwenzi, *Sci. Total Environ.* **2019**, *669*, 785–797.
- [2] A. Tursi, E. Chatzisympson, F. Chidichimo, A. Beneduci, G. Chidichimo, *Int. J. Environ. Res. Public Health* **2018**, *15*, 2419.
- [3] P. Burkhardt-Holm, *Int. J. Water* **2010**, *26*, 477–493.
- [4] T. Zoltan, M. C. Rosales, C. Yadarola, *J. Environ. Chem. Eng.* **2016**, *4*, 3967–3980.
- [5] M. Rosales, T. Zoltan, C. Yadarola, E. Mosquera, F. Gracia, A. García, *J. Mol. Liq.* **2019**, *281*, 59–69.
- [6] J. Matos, M. Rosales, A. García, C. Nieto-Delgado, J. R. Rangel-Mendez, *Green Chem.* **2011**, *13*, 3431–3439.
- [7] R. Prasad, *Advanced Research in Nanosciences for Water Technology*, **2019**.
- [8] P. G. Saiz, A. Valverde, B. Gonzalez-Navarrete, M. Rosales, Y. M. Quintero, A. Fidalgo-Marijuan, J. Orive, A. Reizabal, E. S. Larrea, M. I. Arriortua, S. Lanceros-Méndez, A. García, R. Fernández de Luis, R. Gonçalves, M. M. Silva, S. Wuttke, A. Fidalgo-Marijuan, C. M. Costa, J. L. Vilas-Vilela, J. M. Laza, M. I. Arriortua, S. Lanceros-Méndez, R. Fernández de Luis, *Catal.* **2020**, *11*, 11907–11919.
- [9] Z. Dong, Y. Sun, J. Chu, X. Zhang, H. Deng, *J. Am. Chem. Soc.* **2017**, *139*, 14209–14216.
- [10] Q. Liu, Y. Song, Y. Ma, Y. Zhou, H. Cong, C. Wang, J. Wu, G. Hu, M. O’Keeffe, H. Deng, *J. Am. Chem. Soc.* **2019**, *141*, 488–496.
- [11] A. Reizabal, C. M. Costa, P. G. Saiz, B. Gonzalez, L. Pérez-Álvarez, R. Fernández de Luis, A. García, J. L. Vilas-Vilela, S. Lanceros-Méndez, *J. Hazard. Mater.* **2021**, *403*, 123675.
- [12] J. A. González, M. E. Villanueva, L. L. Piehl, G. J. Copello, *Chem. Eng. J.* **2015**, *280*, 41–48.
- [13] M. E. Villanueva, A. M. D. R. Diez, J. A. González, C. J. Pérez, M. Orrego, L. Piehl, S. Teves, G. J. Copello, *ACS Appl. Mater. Interfaces* **2016**, *8*, 16280–16288.
- [14] J. A. González, M. E. Villanueva, M. L. Peralta Ramos, C. J. Pérez, L. L. Piehl, G. J. Copello, *RSC Adv.* **2015**, *5*, 63813–63820.
- [15] M. E. Villanueva, A. Salinas, L. E. Díaz, G. J. Copello, *New J. Chem.* **2015**, *39*, 614–620.
- [16] H. Reinsch, S. Waitschat, S. M. Chavan, K. P. Lillerud, N. Stock, *Eur. J. Inorg. Chem.* **2016**, 4490–4498.
- [17] A. E. Baumann, D. A. Burns, B. Liu, V. S. Thoi, *Commun. Chem.* **2019**, *2*, 86.
- [18] P. G. Saiz, G. Gandia, A. Lasheras, A. Sagasti, I. Quintana, M. L. Fdez-Gubieda, J. Gutiérrez, M. I. Arriortua, A. C. Lopes, *Sens. Actuators B* **2019**, *296*, 126612.
- [19] P. G. Saiz, N. Iglesias, B. Gonzalez-Navarrete, M. Rosales, Y. M. Quintero, A. Reizabal, J. Orive, A. Fidalgo-Marijuan, S. Lanceros-Mendez, M. I. Arriortua, R. Fernandez de Luis, *Chem. Eur. J.* **2020**, *26*, 13861–13872.
- [20] H. Li, M. Eddaoudi, M. O’Keeffe, O. M. Yaghi, *Nature* **1999**, *402*, 276–279.
- [21] G. Maurin, C. Serre, A. Cooper, G. Férey, *Chem. Soc. Rev.* **2017**, *46*, 3104–3107.
- [22] M. Mon, F. Lloret, J. Ferrando-Soria, C. Martí-Gastaldo, D. Armentano, E. Pardo, *Angew. Chem. Int. Ed.* **2016**, *55*, 11167–11172; *Angew. Chem.* **2016**, *128*, 11333–11338.
- [23] S. Yuan, J. S. Qin, C. T. Lollar, H. C. Zhou, *ACS Cent. Sci.* **2018**, *4*, 440–450.
- [24] M. S. Denny, S. M. Cohen, *Angew. Chem. Int. Ed.* **2015**, *54*, 9029–9032; *Angew. Chem.* **2015**, *127*, 9157–9160.
- [25] D. Feng, K. Wang, Z. Wei, Y. P. Chen, C. M. Simon, R. K. Arvapally, R. L. Martin, M. Bosch, T. F. Liu, S. Fordham, D. Yuan, M. A. Omary, M. Haranczyk, B. Smit, H. C. Zhou, *Nat. Commun.* **2014**, *5*, 5723.
- [26] C. Wang, X. Liu, N. Keser Demir, J. P. Chen, K. Li, *Chem. Soc. Rev.* **2016**, *45*, 5107–5134.
- [27] O. M. Yaghi, M. O’Keeffe, N. W. Ockwig, H. K. Chae, M. Eddaoudi, J. Kim, *Nature* **2003**, *423*, 705–714.
- [28] B. Illes, S. Wuttke, H. Engelke, *Nanomaterials* **2017**, *7*, 351.
- [29] B. Steinborn, P. Hirschle, M. Höhn, T. Bauer, M. Barz, S. Wuttke, E. Wagner, U. Lächelt, *Adv. Ther.* **2019**, *2*, 1900120.
- [30] D. Wisser, F. M. Wisser, S. Raschke, N. Klein, M. Leistner, J. Grothe, E. Brunner, S. Kaskel, *Angew. Chem. Int. Ed.* **2015**, *54*, 12588–12591; *Angew. Chem.* **2015**, *127*, 12776–12780.
- [31] D. Zhou, L. Zhang, J. Zhou, S. Guo, *Water Res.* **2004**, *38*, 2643–2650.
- [32] D. I. Torres, J. M. Lazaro-Martínez, G. J. Copello, V. C. dall Orto, *J. Environ. Chem. Eng.* **2019**, 103416.
- [33] R. Jayakumar, M. Prabakaran, P. T. Sudheesh Kumar, S. V. Nair, H. Tamura, *Biotechnol. Adv.* **2011**, *29*, 322–337.
- [34] R. Jayakumar, D. Menon, K. Manzoor, S. V. Nair, H. Tamura, *Carbohydr. Polym.* **2010**, *82*, 227–232.
- [35] X. Shen, J. L. Shamshina, P. Berton, G. Gurau, R. D. Rogers, *Green Chem.* **2015**, *18*, 53–75.
- [36] J. Araki, Y. Yamanaka, K. Ohkawa, *Polym. J.* **2012**, *44*, 713–717.
- [37] E. Ruckenstein, X. Zeng, *J. Membr. Sci.* **1998**, *142*, 13–26.
- [38] A. H. Brown, T. R. Walsh, *ACS Biomater. Sci. Eng.* **2019**, *5*, 594–602.
- [39] M. Yahyaei, F. Mehrnejad, H. Naderi-manesh, A. H. Rezayan, *Carbohydr. Polym.* **2018**, *191*, 191–197.
- [40] P. Taylor, R. N. Tharanathan, F. S. Kittur, *Crit. Rev. Food Sci. Nutr.* **2003**, *43*, 61–87.
- [41] P. A. Felse, T. Panda, *Bioprocess Eng.* **1999**, *20*, 505–512.
- [42] J. Jiang, F. Gándara, Y. B. Zhang, K. Na, O. M. Yaghi, W. G. Klemperer, *J. Am. Chem. Soc.* **2014**, *136*, 12844–12847.
- [43] S. Lin, Y. Zhao, J. K. Bediako, C. Cho, A. K. Sarkar, C. Lim, Y. Yun, *Chem. Eng. J.* **2019**, *362*, 280–286.
- [44] C. Wang, X. Liu, J. P. Chen, K. Li, *Sci. Rep.* **2015**, *5*, 16613.
- [45] Z. Q. Li, J. C. Yang, K. W. Sui, N. Yin, *Mater. Lett.* **2015**, *160*, 412–414.
- [46] T. Stassin, H. Reinsch, B. Van de Voorde, S. Wuttke, D. D. Medina, N. Stock, T. Bein, R. Ameloot, D. De Vos, *ChemSusChem* **2017**, *10*, 643–650.
- [47] A. Valverde, R. Gonçalves, M. M. Silva, S. Wuttke, A. Fidalgo-Marijuan, C. M. Costa, J. L. Vilas-Vilela, J. M. Laza, M. I. Arriortua, S. Lanceros-Méndez, R. Fernández de Luis, *ACS Appl. Mater. Interfaces* **2020**, *3*, 12, 11907–11919.
- [48] S. Rojas, P. Horcajada, *Chem. Rev.* **2020**, *120*, 8378–8415.
- [49] M. Mon, R. Bruno, J. Ferrando-Soria, D. Armentano, E. Pardo, *J. Mater. Chem. A* **2018**, *6*, 4912–4947.
- [50] N. Stock, S. Biswas, *Chem. Rev.* **2012**, *112*, 933–969.
- [51] Z. Hu, I. Castano, S. Wang, Y. Wang, Y. Peng, Y. Qian, C. Chi, X. Wang, D. Zhao, *Cryst. Growth Des.* **2016**, *16*, 2295–2301.
- [52] Y. Chen, X. Huang, S. Zhang, S. Li, S. Cao, X. Pei, J. Zhou, X. Feng, B. Wang, *J. Am. Chem. Soc.* **2016**, *138*, 10810–10813.
- [53] H. Furukawa, F. Gándara, Y. B. Zhang, J. Jiang, W. L. Queen, M. R. Hudson, O. M. Yaghi, *J. Am. Chem. Soc.* **2014**, *136*, 4369–4381.
- [54] J. Baek, B. Rungtaweeworanit, X. Pei, M. Park, S. C. Fakra, Y. S. Liu, R. Matheu, S. A. Alshimri, S. Alshehri, C. A. Trickett, G. A. Somorjai, O. M. Yaghi, *J. Am. Chem. Soc.* **2018**, *140*, 18208–18216.
- [55] P. Sikorski, R. Hori, M. Wada, *Biomacromolecules* **2009**, *10*, 1100–1105.
- [56] A. H. Valekar, S. G. Lee, K. H. Cho, U. H. Lee, J. S. Lee, J. W. Yoon, Y. K. Hwang, S. J. Cho, J. S. Chang, *RSC Adv.* **2017**, *7*, 55767–55777.
- [57] H. V. Doan, H. Amer Hamzah, P. Karikkethu Prabhakaran, C. Petrillo, V. P. Ting, *Hierarchical Metal-Organic Frameworks with Macroporosity: Synthesis, Achievements, and Challenges*, Springer Singapore, **2019**.
- [58] M. M. Modena, B. Rühle, T. P. Burg, S. Wuttke, *Adv. Mater.* **2019**, *31*, 1901556.
- [59] H. Zhang, Y. Zhao, *Food Hydrocolloids* **2015**, *48*, 260–273.
- [60] K. Suhailath, P. Jayakrishnan, B. Naufal, P. Periyat, V. C. Jasna, M. T. Ramesan, *Adv. Polym. Technol.* **2018**, *37*, 1114–1123.

- [61] D. Xie, Y. Ma, Y. Gu, H. Zhou, H. Zhang, G. Wang, Y. Zhang, H. Zhao, *J. Mater. Chem. A* **2017**, *5*, 23794–23804.
- [62] J. Luo, F. Xu, J. Hu, P. Lin, J. Tu, X. Wu, X. Hou, *Microchem. J.* **2017**, *133*, 441–447.
- [63] M. Sarker, J. Y. Song, S. H. Jhung, *J. Hazard. Mater.* **2017**, *335*, 162–169.
- [64] A. Maleki, B. Hayati, M. Naghizadeh, S. W. Joo, *J. Ind. Eng. Chem.* **2015**, *28*, 211–216.
- [65] J. de Decker, J. de Clercq, P. Vermeir, P. van der Voort, *J. Mater. Sci.* **2016**, *51*, 5019–5026.
- [66] Z. J. Lin, H. Q. Zheng, H. Y. Zheng, L. P. Lin, Q. Xin, R. Cao, *Inorg. Chem.* **2017**, *56*, 14178–14188.
- [67] P. G. Saiz, A. Valverde, B. Gonzalez-Navarrete, M. Rosales, Y. M. Quintero, A. Fidalgo-Marijuan, J. Orive, A. Reizabal, E. S. Larrea, M. I. Arriortua, S. Lanceros-Méndez, A. García, R. Fernández de Luis, *Catalysis* **2021**, *11*, 51.
- [68] Z. Wang, J. Yang, Y. Li, Q. Zhuang, J. Gu, *Chem. Eur. J.* **2017**, *23*, 15415–15423.
- [69] A. Gallardo-Godoy, K. A. Hansford, C. Muldoon, B. Becker, A. G. Elliott, J. X. Huang, R. Pelingon, M. S. Butler, M. A. T. Blaskovich, M. A. Cooper, *Molecules* **2019**, *24*, 533.
- [70] F. Lu, D. Astruc, *Coord. Chem. Rev.* **2020**, *408*, 213180.
- [71] K. Liang, R. Ricco, C. M. Doherty, M. J. Styles, S. Bell, N. Kirby, S. Mudie, D. Haylock, A. J. Hill, C. J. Doonan, P. Falcaro, *Nat. Commun.* **2015**, *6*, 4–11.
- [72] A. J. Howarth, M. J. Katz, T. C. Wang, A. E. Platero-Prats, K. W. Chapman, J. T. Hupp, O. K. Farha, *J. Am. Chem. Soc.* **2015**, *137*, 7488–7494.
- [73] S. J. Allen, G. Mckay, J. F. Porter, *J. Colloid Interface Sci.* **2004**, *280*, 322–333.
- [74] N. C. Burtch, H. Jasuja, K. S. Walton, *Chem. Rev.* **2014**, *114*, 10575–10612.
- [75] J. Jiang, F. Gándara, Y. B. Zhang, K. Na, O. M. Yaghi, W. G. Klemperer, *J. Am. Chem. Soc.* **2014**, *136*, 12844–12847.
- [76] H. Furukawa, F. Gándara, Y. B. Zhang, J. Jiang, W. L. Queen, M. R. Hudson, O. M. Yaghi, *J. Am. Chem. Soc.* **2014**, *136*, 4369–4381.
- [77] J. A. González, M. E. Villanueva, M. L. Peralta Ramos, C. J. Pérez, L. L. Piehl, G. J. Copello, *RSC Adv.* **2015**, *5*, 63813–63820.

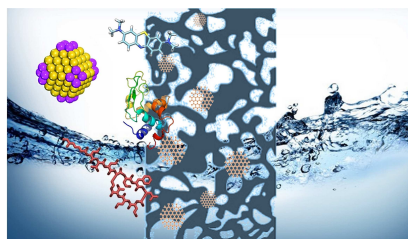
Manuscript received: April 1, 2021

Accepted manuscript online: April 8, 2021

Version of record online: ■■■, ■■■■

FULL PAPERS

Clean it up: Chitin (CH) macro- and mesoporous biopolymer and metal-organic framework (MOF) microporous nanoparticles are combined to obtain a macro- to microporous sorbent able to retain pollutants from the Ångstrom to nanometer scales. CH/MOF composites outperform the adsorption capacities of the average sum of their CH and MOF components due to their improved textural properties and diverse surface chemistry effects.



G. I. Tovar Jimenez, A. Valverde, C. Mendes-Felipe, Prof. S. Wuttke, Dr. A. Fidalgo-Marijuan, Dr. E. S. Larrea, Prof. L. Lezama, F. Zheng, Dr. J. Reguera, Prof. S. Lanceros-Méndez, Prof. M. I. Arriortua, Dr. G. Copello*, Dr. R. F. de Luis**

1 – 11

**Chitin/Metal-Organic Framework
Composites as Wide-Range
Adsorbent**

